Structure of alluvial valleys from 3-D gravity inversion: The Low Andarax Valley (Almería, Spain) test case

Antonio G. Camacho[1], Enrique Carmona[2,3], Antonio García-Jerez[3], Francisco Sánchez-Martos[4], Juan F. Prieto[5], José Fernández[1], Francisco Luzón[2,3]

[1]Instituto de Geociencias (CSIC-UCM), Facultad CC. Matemáticas, Plaza de Ciencias, 3. Ciudad Universitaria, 28040-Madrid. (antonio_camacho@mat.ucm.es)

[2]Dpto de Química y Física, Universidad de Almería, Cañada de San Urbano s/n, 04120-Almería.

[3]Instituto Andaluz de Geofísica, Universidad de Granada, Campus Universitario de Cartuja, 18071 Granada.

[4]Dpto de Biología y Geología, Universidad de Almería, Cañada de San Urbano s/n, 04120-Almería.

[5]Dpto de Ingeniería Topográfica y Cartografía, ETSI Topografía, Geodesia y Cartografía, Universidad Politécnica de Madrid, Km 7.5 Autovía de Valencia, 28031-Madrid.

1

Abstract

This paper presents a gravimetric study (based on 382 gravimetric stations in an area about 32 km^2) of a nearly flat basin: the Low Andarax valley. This alluvial basin, close to its river mouth, is located in the extreme south of the province of Almería and coincides with one of the existing depressions in the Betic Cordillera. The paper presents new methodological work to adapt a published inversion approach (GROWTH method) to the case of an alluvial valley (sedimentary stratification, with density increase downward). The adjusted 3D density model reveals several features in the topography of the discontinuity layers between the calcareous basement (2700 kg/m^3) and two sedimentary layers (2400 kg/m^3 and 2250 kg/m^3). We interpret several low density alignments as corresponding to SE faults striking about N 140-145ºE. Some detected basement elevations (as one, previously known by boreholes, in Viator village) are apparently connected with the fault pattern. The outcomes of this work are: (1) new gravimetric data, (2) new methodological options, and (3) resulting structural conclusions.

1. Introduction

The inverse gravimetric problem, namely the determination of a subsurface mass density distribution corresponding to an observed gravity anomaly, has an intrinsic non-uniqueness in its solution (e.g. Al-Chalabi 1971). Nevertheless, particular solutions can be obtained by including additional constraints on the model (geometry of the subsurface structure) and on the data parameters (statistical properties of the inexact data, e.g. Gaussian distribution of errors).

The shallow basin structures filled with light sedimentary material constitute a particularly interesting case of the gravity inversion, due to their geological interest. They cause a closed negative anomaly, which usually is modelled by considering an outcroppoing flat low-density body (homogeneous or stratified) limited by a concave shallow bottom. (e.g. Leao *et al*. 1996). The usual inversion methods look for determining, in a non-linear approach, the bottom interface as defined by elementary cells. Rectangular prisms have been used widely to describe the model structure (eg. Cordell and Henderson, 1968; Rama Rao et al., 1999).

The case of assuming a subsurface structure characterised by several sub-horizontal layers of prescribed density contrasts is more complex and involves a higher ambiguity. The main problem is to assign the features of the anomaly map as produced by irregularities on one or another interface. Traditional methodologies are mostly based on the calculation of the Fourier transform of the gravitational anomaly as the sum of the Fourier transform of powers of the perturbing interface topographies (e.g. Oldenburg, 1974; Chakraborty and Agarwal, 1992; Reamer and Ferguson, 1989).

Camacho et al. (2009 and 2011a) describe a general method and a code ("GROWTH") to carry out a 3D gravity inversion in a non-subjective approach, able to determine the

geometry of the causative bodies. Camacho et al. (2011b) proposed a modification of the original methodology enabling to deal with isolated bodies or stratified structures in a versatile form. The key idea is to modify the adjustment equations for isolated bodies (GROWTH method) by adding a weighting matrix enabling to shift of the adjusted anomalous masses closer to the discontinuity interfaces.

In the present paper we describe a new alternative possibility of obtaining stratified structures by means of the GROWTH methodology. The key idea is to change the prescribed density contrast at some stage during the growing process of modelling. It is combined with a suitable choice of the gravity constant offset. These new options allow modeling stratified structures as, for instance, alluvial valleys by means of 3D models. It will provide interesting results concerning the topography of the discontinuity surfaces, the presence of large faults, and the existence of particular anomalous bodies included. This type of geological structures are composed fundamentally by sedimentary rocks and represent the material record in the form of rock layers or strata that once existed on the earth. Sedimentary rocks contain information about what earth surface environments were like in the past and can contain important natural resources. From the seismic engineering point of view, sedimentary materials can produce the so-called local seismic effects, generating the amplification of the seismic inputs and spectral resonances at the free surface of an alluvial valley (see e.g. Luzón et al., 1995, 2004, 2009).

As a test example, the proposed gravity inversion approach is applied to a data set recently collected for studying the Low Basin of the River Andarax in the Betic Cordillera. This area is one of the most arid regions in Europe with very irregular precipitation. The intensive agricultural activity depends on the exploitation of the groundwater. We aim to determine a model of the subsurface mass distribution composed by some irregular strata.

4

2. Geological setting.

The tectonically active Betic Cordillera is a topographic manifestation of the collision between the African and Iberian plates. It consists of E–W and NE–SW trending mountain ranges separated by less elevated sedimentary basins. Betic basins were marine depocenters from late Miocene through Pliocene time, and emergent until upper Pliocene/ lower Pleistocene time (Sanz de Galdeano and Vera, 1992)

The Low Basin of the River Andarax is located in the extreme south of the province of Almeria (Fig. 1) and coincides with one of the existing depressions in the Betic Cordillera. This valley, which is limited to the south by the Mediterranean Sea, is enclosed by Sierra Alhamilla (in the East), with its mainly metapelitic outcrops, and Sierra de Gádor (in the West), which constitutes a carbonate-dolomite massif with outcroppings of phyllites (Fig. 1). The depression is filled by post-orogenic detrital deposits of diverse lithology (marls, sandy silts, sands and conglomerates) with evaporite intercalations of gypsiferous nature. The mica-schists and quartzites are practically impervious, while the carbonate formation has high porosity and permeability values due to fissures and/or karstification. The post-orogenic rocks exhibit great differences in permeability. The Miocene and Pliocene marly formations have very low permeability, whereas the Pliocene deltaic sediments and the Quaternary and Plio-quaternary formations are water-bearing. In accordance with this distribution, three hydrogeological units have been defined: Detrital Aquifer, Carbonate Aquifer and Deep Aquifer (Pulido-Bosch et al., 1991; Sánchez-Martos, 1997).

FIGURE 1

The Low Andarax basin corresponds to an alluvial valley of about 250 km^2. It is located in one of the most arid regions in Europe, which is characterized by its low (200 - 350 mm/

year) and irregular precipitation which falls mainly (70%) in autumn and winter (Martín-Rosales et al., 1996). This determines the pattern of groundwater exploitation supporting an intensive agricultural activity.

This basin is situated in an active seismic region, with the highest seismic hazard values in Spain, where shallow seismic series occur frequently (in fact, the valley is encircled by very near active faults systems). The intense tectonic activity of the zone (Sanz de Galdeano *et al.*, 1985) favours an important geothermal activity, as demonstrated by the thermal springs of the Sierra Alhamilla (51.8 ºC) and Alhama (40.8 ºC). The tectonic activity of the area has affected the relationship between the different aquifer units. The main late Miocene to Quaternary tectonic structures in the southwestern side of the Alhamilla ridge, in the Almería-Níjar basin are Pliocene-Quaternary high-angle normal faults striking NW-SE to NNW-SSE strike (Martínez-Martínez and Azañón, 1997). The fractures coincide with old faults from the Miocene period and have been reactivated during the Quaternary, with throws not higher than 10 m (Voermans and Baena, 1983). These faults present many young echeloned scarps to the SW of Sierra Alhamilla. (Sanz de Galdeano et al., 2010). The NW-SE striking fractures show a great influence on the topography, and are interpreted as deformations in the surface linked to a movement in depth conjugated to the Carboneras fault (Pedrera et al., 2006).

Moreover, the seismic hazard is also reinforced because the landform is mainly composed of sedimentary materials which produce the so-called local seismic effects, with the amplification of the seismic inputs and spectral resonances in the free surface of the valley.

Considering all those problems and characteristics, we aim to get new information about the sub-surface 3D density structure of the Low Andarax valley by using new geophysical data and new inversion methodology.

3. Methodology

We present in this section: (1) a brief description of the methodological principles of the previously published methodology for free inversion of isolated 3D bodies, and, (2), the modified version to account for the characteristics of basin structures with several discontinuity interfaces representing alluvial valleys environments.

3.1 General approach

Large parts of the basic inversion methodology and associated mathematical concepts are described in Camacho et al. (2009, 2011a, b). We therefore summarize the key concepts here.

Suppose a data set constitutes of gravity values observed at n gravity benchmarks, irregularly distributed. Let (x_i,y_i,z_i), $i=1,...,n$, be the planar coordinates (UTM coordinates) and the altitudes of the gravity stations P_i and let Δg_i, be the respective gravity anomaly (Bouguer gravity anomaly). We must consider the gravity data as imprecise values whose uncertainties show Gaussian distribution, characterised by a covariance (n,n)-matrix, Q_D. Usually, we set $q_{ij}= 0$, for i$\neq$j, and $q_{ii}= e_i^2$, where e_i, $i=1,...,n$, are standard deviations of the gravity values.

The inversion process constructs a subsurface model defined by a 3-D aggregation of m parallelepiped cells, which are filled, in a "growth" process, by means of prescribed positive and negative density contrasts. The design equation to relate observables, i.e. the gravity anomaly Δg_i at n benchmarks (x_i,y_i,z_i), with modelling parameters and residuals v_i is:

$$\Delta g_i = \sum_{j \in J^+} A_{ij}\Delta\rho_j^+ + \sum_{j \in J^-} A_{ij}\Delta\rho_j^- + dg_{reg} + v_i \quad , \quad i=1,...,n \quad , \tag{1}$$

where A_{ij} is the vertical attraction for unit density for the j-th parallelepiped cell upon the i-th observation point (e.g., Pick et al., 1973), $\Delta\rho_j^-$, $\Delta\rho_j^+$ are prescribed density contrasts (negative

and positive fixed values) for the j-th cell, J^+, J^- are sets of indexes corresponding to the cells filled with positive or negative density values, and δg_{reg} is a regional component composed of an offset regional value g_0 and a linear trend:

$$\delta g_{reg} = g_0 + g_x(x_i - x_M) + g_y(y_i - y_M) \quad , \quad i = 1,...,n \tag{2}$$

x_M and y_M are average coordinates for the survey area, g_x, g_y are unknown values for the horizontal gravity gradients.

Sets J^+ and J^- constitute the main unknown to be determined in the inversion approach. They design cells filled with positive and negative density contrast, then determining the geometry of the anomalous bodies in a non-linear relationship.

Following the general treatment of the least-squares inversion methods of Tarantola (1988), to solve the problem of non-uniqueness, we adopt a mixed minimization condition, based on model "fitness" (least square minimization of residuals) and model "smoothness" (l_2-minimization of total anomalous mass)

$$\boldsymbol{v}^T \boldsymbol{Q}_D^{-1} \boldsymbol{v} + \lambda \ \boldsymbol{m}^T \boldsymbol{Q}_M^{-1} \boldsymbol{m} = \min, \tag{3}$$

where $\boldsymbol{m} = (\Delta\rho_{1_1},...,\Delta\rho_m)^T$ (superscript T denotes transpose of a matrix) are density contrast values for the m cells of the model, $\boldsymbol{v} = (v_1,...,v_n)^T$ are residual values for the n data points, $\boldsymbol{Q}_D$ is an a priori covariance matrix for uncertainties of the gravity data, $\boldsymbol{Q}_M$ is an a priori covariance matrix for uncertainties of the model parameters, and λ is a factor for selected balance between fitness and smoothness of the model. For a problem without prior information about the model structure (Camacho et al., 1997), we suggest to take a model covariance matrix $\boldsymbol{Q}_M$ given by a diagonal normalizing matrix of non-null elements that are

the same as the diagonal elements of $A^T Q_D^{-1} A$. This covariance matrix allows getting inversion models located on suitable depths (see simulation tests in references), and it plays the role of the depth weighting functions in the bibliography about gravity and magnetic data inversion (for instance Li and Oldenburg 1998)

The problem of non-linearity of the system, with a large number of unknowns, is solved by a particular constructive process: The anomalous structures are formed by a nearly homogenous growth by cell addition, from previously adjusted "skeletal" structures, until the bodies attain a suitably developed size. The prismatic cells are systematically tested, step by step, with each prescribed density contrast, and then the best solution is adopted to grow anomalous bodies. The minimization fit conditions are applied for each growth step, and include a scale factor f which relates the immature model to the global conditions concerning gravity fit and model size (mass and volume).

In practice, for an arbitrary $(k+1)$-th step, k prisms have been previously filled with the positive or negative fixed contrast values and the modelled gravity values will be g_i^c, $i=1,...,n$. Now, the process looks, throughout the m-k unchanged prisms, for one new prism to be modified. For that, for each j-th unchanged prism, and for both the negative and positive prescribed density contrasts, the following equation system is considered:

$$g_i - (g_i^c + A_{ij} \Delta\rho_j) f - g_0 - g_x(x_i - x_M) - g_y(y_i - y_M) = v_i \ , i = 1,...,n \quad , \qquad (4)$$

$$v^T Q_D^{-1} v + \lambda f^2 m^T Q_M^{-1} m = \min., \qquad (5)$$

where $\Delta\rho_j$ are the prescribed values $\Delta\rho_j^+$ and $\Delta\rho_j^-$, and $f \geq 1$ is an unknown scale factor for fitting the modelled anomalies $(\Delta g_i^c + A_{ij}\Delta\rho_j)$ to the observed anomalies (Δg). Then, the

unknown parameters f, g_x and g_y are adjusted by solving the system (4) and (5), where the vector m of solutions now includes the values for the previously filled cells and the value $\Delta\rho_j$ that is being tested. Once the former linear equations have been solved, we can calculate the misfit value e_j^2 defined by

$$e_j^2 = \boldsymbol{v}^T \boldsymbol{Q}_D^{-1} \boldsymbol{v} + \lambda \, f^2 \, \boldsymbol{m}^T \boldsymbol{Q}_M^{-1} \boldsymbol{m}$$

(6)

as the parameter for the suitability of the j-th prism and the adopted density contrast (positive $\Delta\rho_j^+$ or negative $\Delta\rho_j^-$). Then, the j-th prism with a density contrast producing a minimum value of e_j^2 is selected to grow the anomalous body, adding its effect to the modelled Δg_i^c values (see Camacho et al., 2007, for details).

This process is repeated in a step-wise manner until a best fitting model is obtained. For each successive step, the scale value f decreases. The process stops when f approaches 1, resulting in the modelled 3-D structure for anomalous density and a final linear regional trend. Camacho et al. (2000 and 2002) and Gottsmann et al. (2008) give some simulation examples showing the suitability of this 3D inversion approach while also pointing out some limitations.

For isolated anomalous bodies we suggest to include the parameter g_0 as unknown parameter in the fit equations. The reference papers give details about this option. The adjusted value for g_0 will contribute to satisfy the minimization condition. For isolated bodies we also suggest to keep the same anomalous density contrast ($\Delta\rho^+$ and $\Delta\rho^-$) across the model growth. The resulting anomalous bodies will be homogeneous and comparable among each other.

In the present study we introduce two improvements in the methodology to allow for a suitable modeling of stratified erosional structures, as the case of alluvial valleys. They are:

(a) The adoption of a suitable gravity offset g_0, and (b) The adoption of stepped density contrasts.

3.2 Gravity offset g_0

A value of g0 resulting from a free adjustment according to the global minimization conditions (eq. 4) will be not very different from a mean anomaly value. It will provide isolate anomalous bodies with good fitting. These isolated bodies will involve some depth inverse mass distribution: positive anomalous density upon no-anomalous medium, or negative anomalous density below no-anomalous medium.

For a realistic stratified structure (as the case of a basin) the density follows mostly a non-inverse distribution: density increase with depth. Inverse distributions are possible, but not frequent. We could restrict our results to models with non-inverse density distribution only. And it could be partially controlled with the gravity offset parameter g_0.

For a model cell j with (positive or negative) density contrast $\Delta\rho_j$ located just upon a cell k with (positive, negative or null) density contrast $\Delta\rho_k$, we define the inverse contribution C_j as $C_j = D_j\,S_j$, where $D_j = \Delta\rho_j - \Delta\rho_k$ if $\Delta\rho_j > \Delta\rho_k$ and $D_j = 0$ in other case. S_j is the contact area between j and k cells. The sum of the inverse contributions

$$C = \sum_{j \in J^+, J^-} C_j p_j \bigg/ \sum_j p_j \ , \ \text{with} \ \ p_j = \frac{1}{n}(\sum_{i=1,...,n} dist^2(j-cell, i-benchmark))^{1/2} \qquad (7)$$

gives an index of the mass inversion present in the model. For a value g_0 close to the mean anomaly the model will be constituted mostly by isolated bodies. The index of mass inversion C will be high. If we try smaller g_0 values, the value C will decrease, and the model will offers larger positive masses in the bottom. If, simultaneously, we limit the maximum model depth, the model becomes rather stratified. After some trials, and without another additional information, we can reach a suitable g_0 value that produce $C \approx 0$. The corresponding model will

11

present a suitable mass/depth distribution.

3.3 Stepped density contrasts

Usually, to get homogeneous bodies for the anomalous structures, and without other previous information, we take the prescribed values $\Delta\rho_j^+$ and $\Delta\rho_j^-$ as contant values everywhere and at every time during the computation. Then, the model shows only one value for the anomalous density contrast everywhere. See simulation examples in Camacho et al. (2000 and 2002).

The alternative approach we propose here is to construct models with a higher density contrast in their core (or their bottom, for stratified structures) and with a lighter density contrast for their periphery (or their top, for stratified structures). For that, we start the model growth (Fig. 2) with prescribed density contrasts $\Delta\rho_0^+$ and $\Delta\rho_0^-$ (for instance, 60 kg/m^3 in Figs. 2 and 3). For the adjusted initial cell, the adjusted scale factor takes the value f_0. The growth process continues by adding new filled cells to the anomalous model. The adjusted scale factor decreases rapidly for the initial steps (see Fig. 2). The density contrast remains at their initial values $\Delta\rho_0^+$ and $\Delta\rho_0^-$. When the scale factor arrives at a value f_1, we introduce a new (smaller) density contrast $\Delta\rho_1^+$ (for instance, 30 kg/m^3 in Fig. 2) for the following cells in the model growth. The process continues with this new density contrast. The negative density contrast can change at this point (f_1) or in another independent moment.

FIGURE 2

FIGURE 3

The choice of the suitable value f_1 (or, better, f_1/f_0) for density change will be decided with regard to the resulting model, and according information from boreholes or geologic or seismic data. Fig. 3 shows an example of model (a) with one density contrast (60 kg/m^3), and

(2) with a change of density contrast (form 60 to 30 kg/m^3) at some step in the model growth (according Fig. 2). This concept can be extended to several successive density (decreasing) changes to produce a stratified model with several layers.

3.4 Synthetic example.

In previous papers, (Camacho et al. 2000 and 2002, and Gottsmann et al. 2008) we presented some simulation test examples corresponding to the general GROWTH methodology for gravity inversion. Now, this section shows a brief synthetic example to illustrate the effect of the news (aadoption of a suitable gravity offset, and adoption of stepped density contrasts) corresponding to the study of an alluvial valley.

For higher homogeneity, we suppose the same area and the same distribution of gravity points as in the further application case (Low Andarax Valley, section 4). Below this area we suppose a synthetic valley structure composed by four layers with density contrast -250, 0 250, 500 kg/m^3 and reaching a depth bout 1500 m. See Figure 4. The adopted synthetic value for g_0 is 0 μm/s^2 . Figure 4 b shows the simulated gravity anomaly field corresponding to the synthetic structure.

By means of direct application of the general GROWTH method for gravity inversion, with an only density contrast ±400 kg/m^3 and free adjustment of the gravity offset g_0, the resulting 3D model for anomalous density is that of Fig. 4 c. The corresponding adjusted value for g_0 is 227 μm/s^2. This model could be suitable for other kind of structures (isolate bodies within a rather homogeneous medium), but it is inadequate for a stratified basin context.

FIGURE 4

By application of the gravity inversion approach including the news of this paper (aadoption of a suitable gravity offset, and adoption of stepped density contrasts) and the

same density contrast (-250, 0 250, 500 kg/m^3) the resulting model (Fig. 4d) is clearly advantageous. It shows a stratified basin structure. The value for g_0 is now -37 μm/s^2. With a larger data set (greater coverage upon the anomalous structure) the fit with respect to the synthetic body would be even greater.

4. Application test case: The Low Andarax valley (Almería, Spain)

As test case, this new approach will be applied to get a structural 3D density model from the new gravity data observed in the Low Andarax valley. In the following, we describe the data and the resulting model.

4.1 Data: gravity, positioning and DEM.

The gravimetric survey in the Low Andarax Valley (LAV) was carried out during two field campaigns in July 2012 and May 2013. It consists of 382 gravimetric stations (see Fig. 1) covering the studied area, with a station spacing of about 200 m. A CG-5 Scintrex gravimeter was used for the field measurements. The total number of gravimetric observations was 437. The number of repeated stations was 11 and the number of observations at these base stations was 66.

Simultaneously, by using geodetic GPS TOPCON equipment, we determined the positions of the gravity stations with an accuracy better than ± 5 cm (this would amount to about 0.15 μm/s^2). This GNSS geodetic support of the gravimetric observations was carried out using the Relative-Static method by carrier phase differences (Hoffmann-Wellenhof *et al.*, 2008). It was performed collecting GNSS carrier observations for periods of 10 to 30 minutes, depending on the baseline length, and using two GNSS receivers. One of them remained collecting GNSS data in the same place during all the field campaign while the other one recorded GNSS observations on the gravimetric station simultaneously with the gravimetric

14

observations.

For the GNSS data processing, an existing permanent GNSS station was added to the processing routines, ALME. It is an EUREF station operated by the IGN CORS network (Prieto *et al.*, 2000). GNSS data were processed using International GNSS Service final combined solution precise ephemerides (Dow *et al.*, 2009) and calibration antennae patterns from National Geodetic Survey (Mader and Bilich, 2012). A L3 free fix ambiguity solution was obtained using the Hopfield tropospheric model (Hopfield, 1969). Final coordinates were computed relative to geodetic reference system ETRS89 (European Terrestrial Reference System 1989), which uses GRS80 ellipsoid (Moritz, 1980). The orthometric altitudes were computed from ellipsoid ones using the EGM08-REDNAP geoid model from IGN (IGN, 2010).

This dataset is complemented with a digital elevation model, DEM (Fig. 1), for the surrounding area, with a step of 10 m x 10 m, and extended up to a radius of 20 km around the area (Junta de Andalucía, 2005).

The process of data correction starts with the determination of the tidal correction for the gravity data. The obtained values range between -0.79 and +1.10 $n\mu m/s^2$l. Next, by using a global fit of the redundant observations, we obtained that the precision of the adjusted (relative) gravity values was $\pm$ 0.38 $\mu m/s^2$. The adjusted instrumental drifts accounted for 8.2±0.03 $\mu m/s^2$/day for July 2012 and 6.9±0.09 $\mu m/s^2$/day for May 2013. Next, we carried out a determination of the gravimetric corrections due to terrain effects from the DEM and corresponding to the observation locations. The obtained values range between 264 and 1469 μGal, for a reference terrain density value of 1000 kg/m^3 (This density value is only an initial value that will be changed during the inversion process).

Next, we determined the Bouguer gravity anomaly. First, computation of the normal gravity was referenced to GRS80 (Moritz, 1980). Then, a free-air gradient -3.086 μm/s^2/m. The Bouguer gravity correction was calculated using the average density of 2300 kg/m^3. This local value for average density was determined from the gravity data by looking for a minimum correlation between elevation and gravity anomaly for the shortest wavelength components of topography. It is attained just by means of the further inversion process, according to an improvement developed by Camacho et al. (2007), which allows to modify the initial assumed terrain density.

By including the terrain correction for the gravity disturbances we computed a Bouguer gravity anomaly (with terrain correction). The values of this Bouguer gravity anomaly (with topographic correction) have a dispersion of ± 34.18 μm/s^2, and a difference between extreme values of 225.93 μm/s^2. The corresponding anomaly map (Fig. 5a) shows the dominant presence of a clear ENE-WSW increasing regional trend, which does not allow distinguishing any local details.

FIGURE 5

4.2 Resulting inverse model.

The first result of the inversion process is the simultaneous determination of a linear regional trend (Fig. 5b). In the LAV, this regional trend generates a gravity increase of 18,25 μm/s^2/km according ENE-WSW direction N 51ºE. Casas and Carbó (1990) and Galindo Zaldivar et al. (1997) showed sharp gravity gradients close to the coast in the area of Betics. Torné and Banda (1992) and Galindo Zaldivar (1997) explain these gradients as due to a sharp local change of the crustal thickness. However, this trend can be related with the presence of dense limestones and dolomites of Sierra de Gádor in the western part of the valley

After removing this regional trend, the resulting anomaly (local anomaly) (Fig. 5c) shows some local features, which should correspond to local anomalous density structures. The benchmark elevation values are shown in Fig. 5d. The inversion process uses both data sets to adjust a 3D structure for anomalous density.

The main decision for the gravity inversion is the choice of some density contrast for the model. For that, we follow the previous work by Marín Lechado (2005). He carried out gravimetric studies for two contiguous areas: Campo de Dalías (West) and Campo de Nijar (East). In his wide study he included seismic, magnetic and borehole data, and geologic information. Based on this previous work (mainly in the part of Campo de Dalías), we select the following values to carry out the 3D gravity modelling of the basin: (1) Limy basement: 2700 kg/m^3; (2) intermediate sedimentary infill: 2400 kg/m^3; (3): 2250 kg/m^3; and (4) light deposits: 2000 kg/m^3. So, we include the following anomalous density contrasts +450, +150, 0 ,-250 kg/m^3 for the layered model. Moreover, Marín Lechado (2005) suggested depths for the basement of around 700 m. So we limit our model to a depth of 1.4 km.

Once those parameters are fixed, the inversion approach is nearly automatic. Firtst, we select a 3D grid composed by 83407 cells, with average side about 90 m. The resulting model is determined by a step-by-step aggregation of thousand cells filled with the prescribed density contrasts. It reproduces the observed anomaly well (Fig. 6a). The quality of the adjustment of the model can be assessed from the standard deviation of the final residuals, which is 0.6 μm/s^2 (Fig. 6b). These residuals, essentially uncorrelated, are produced by very local anomalies, slight imperfections in the topographic correction, or the errors in the altimetry or gravimetric observations.

FIGURE 6

Figs. 7 show the resulting 3D model for anomalous density by means of several cross-sections (horizontal sections, and WE and SN vertical profiles). This model shows a stratified structure composed by sub-horizontal layers. Fig.7 suggests the adjusted topography for the discontinuity surfaces S1 and S2 between the assumed media: (M1) +450 kg/m^3 (basement, 2700 kg/m^3), (M2) deep sedimentary infill +150 kg/m^3 (2400 kg/m^3) and (M3) shallow sediments 0 kg/m3 (2250 kg/m^3). Very shallow and light material, M4, - 250 kg/m^3 (2000 kg/m^3) appears only in few locations of the model due to the fact that distance between benchmarks (about 200 m) is larger than the layer thickness of about 100 m (Marín Lechado, 2005). We observe that the adjusted depths amount to about 700 m for S1 (basement) and to about 400 m for S2 (between M2 and M3, Neogene sediments) in the central portion of the low basin. A basement depth of ~550m was estimated in the South of the model in the test-site for the SCA method (García-Jerez, 2010), which shows high densities in that area beneath some interface lying between 400 and 600m.

FIGURE 7

The morphology of the stratified structure mostly corresponds to a nearly flat low basin. However, depths of discontinuity surfaces oscillate showing a topography of lows and highs, suggesting some particular features, which could be correlated with structural peculiarities.

5. Discussions and conclusions

The morphology of the Low Andarax Valley consists of a stratified structure composed by sub-horizontal layers, mostly corresponding to a nearly flat low basin. In the prospected area, the basement is found symmetrically to the river bed, being associated with the foothills of Sierra Alhamilla (eastern edge) and Sierra the Gádor (western edge). The near-surface sections (200 - 300 m) show a more heterogeneous density distribution that may correspond to greater variations in lithologies. Conversely, deeper densities become more uniform,

18

meaning less diverse materials.

We detect a sharp structure of low density in most northern part of the gravity survey. It includes a deep hole in the basement filled by sediments. This is in agreement with the geological data by Marín Lechado (2005) (Figure 8) showing the sedimentary basin fill (marls, silt sands and conglomerates) thickening to the north, and also with data from ground water wells (Sanchez-Martos ,1997). Nevertheless, we would need to extend the gravity survey to the North in future works to get a full coverage of this low and avoid the boundary effects which may distort the anomaly.

FIGURE 8

Some particular features have been inferred from the gravity data. For instance, we observe a particular crest (**V** en Fig. 9) of the layers, close to the village of Viator. This feature agrees with boreholes data and seismic noise surveys, which show a limestone-dolomitic mass at ~200 m depth and a high-density anomaly. This place (near Viator village) is the only zone where boreholes shown in Fig. 9a reveal such type of geological materials. This anomaly, which can be clearly seen in the 200 to 600 meters depth sections, matches previous cross-sections proposed by Sanchez- Martos (1997) on the basis of borehole data. We have found a NW-SE trend for this anomaly and an approximate length of 2 km in horizontal sections down to 500m depth. The model provides new information about similar structures located SE from anomaly V and east of the river channel. These areas have not been sufficiently explored with boreholes or they are very shallow. These anomalies are deeper than Viator structure, being detected below a depth of 500 m.

FIGURE 9

19

Another interesting feature corresponds to certain structural alignments (lows) appreciated in the model for the basin. If we compare this map of alignments with a map of apparent faults in the area (Fig. 8a, Marín Lechado, 2005) some coincidence can be detected. It allows us to interpret these sharp model alignments as corresponding mostly to faults striking mainly NNW-SSE. Fig. 10 shows they run on a horizontal profile obtained by inversion with the general GROWTH inversion method. Alignments following the NW -SE faults can be seen in these sections, according to the NNW –SSE normal faults shown by some authors (Sanz de Galdeano *et al.* 2010; Pedrera *et al.*, 2012). This N 140-160 E direction also coincides with old faults that occurred during the Miocene period (Martínez-Martínez and Azañón, 1997). The alignment N140ºE close to Sierra de Gádor foothills (NW of the prospected area) is the clearest one. It is also interesting to point out that the adjusted gravity regional trend follows the orthogonal course (51ºN). This coincidence suggests some structural relation. Cross-sections of the density model also show probable SSW- NNE trends that have not been described in former works.

FIGURE 10

Acknowledgments

References

Al-Chalabi, M. (1971), Some studies relating to non-uniqueness in gravity and magnetic inverse problem, Geophysics, 36, 835–855, doi:10.1190/ 1.1440219.

Barbosa, V.C.F.; Silva, J.B.C. & Medeiros, W.E. (1997). Gravity inversion of basement relief using approximate equality constraints on depths. *Geophysics*, 62, 1745-1757.

Camacho, A.G., Montesinos, F.G. & Vieira, R. (2000). A 3-D gravity inversion by means of growing bodies. *Geophysics*, 65: 95-101.

Camacho, A.G., Montesinos, F.G. & Vieira, R. (2002). A 3-D gravity inversion tool based on exploration of model possibilities. *Comput. Geosci,* 28, 191-204.

Camacho, A.G., Nunes, J.C., Ortiz, E., França, Z. & Vieira, R. (2007). Gravimetric determination of an intrusive complex under the island of Faial (Azores). Some methodological improvements. *Geophys. J. Int*. 171, 478–494.

Camacho, A.G., Fernández, J., González, P.J., Rundle, J.B., Prieto, J.G., Arjona, A. (2009). Structural results for La Palma Island using 3-D gravity inversion. Journal of Geophysical Research, 114, B05411, doi: 10.1029/2008JB005628.

Camacho, A.G., Fernández, J. & Gottsmann, J. (2011b). A new gravity inversion method for multiple sub-horizontal discontinuity interfaces and shallow basins. *J. Geophys. Res.*, 116, B02413, doi:10.1029/2010JB008023.

Camacho, A.G., Gottsmann, J. & Fernández, J. (2011a). The 3-D gravity inversion package GROWTH2.0 and its application to Tenerife Island, Spain. *Comput. Geosci*, 37 (2011) 621–633.

Casas, A & Carbó, A. (1990). Deep structure of the Betic Cordillera derived from the interpretation of a complete Bouguer anomaly map. J. Geodynamics, 12 (2-4), 137-147.

Chakraborty, K., and B. N. P. Agarwal (1992), Mapping of crustal discontinuities by wavelength filtering on the gravity field, Geophys. Prospect., 40, 801–822, doi:10.1111/j.1365-2478.1992.tb00553.x.

Cordell, L. & Henderson, R. G. (1968). Iterative three-dimensional solution of gravity anomaly data using a digital computer, *Geophysics*, 33, 596–601, doi:10.1190/1.1439955

Dow, J., Neilan, R. E. and Rizos, C. (2009). "The International GNSS Service in a changing landscape of Global Navigation Satellite Systems". Journal of Geodesy, 83(3-4), pp. 191-198.

García-Jerez, A. (2010) Desarrollo y evaluación de métodos avanzados de exploración sísmica pasiva. Aplicación a estructuras geológicas locales del sur de España". PhD. Thesis, Universidad de Almería, Spain.

García-Jerez, A., A. Jiménez, A.J. González-Camacho, E. Carmona, J. Prieto y F. Luzón (2014). Geophysical models at the Andarax River Valley (SE Spain) from ambient seismic noise and microgravimetry, *Procc. of the 8th Asamblea Hispano Portuguesa de Geodesia y Geofisica*, 29-31 January, Evora (Portugal).

Galindo-Zaldívar, J., Jabaloy, A., González-Lodeiro, F., Aldaya, F., (1997). Crustal structure of the central Betic Cordillera (SE Spain). *Tectonics* 16, 18– 37.

Gottsmann, J., Camacho, A.G., Marti, J., Wooller, L., Fernández, J., Garcia, A. & Rymer, H. (2008). Shallow structure beneath the Central Volcanic Complex of Tenerife from new gravity data: Implications for its evolution and recent reactivation. *Phys. Earth Planet. Int.*, 168, 212-230.

Hofmann-Wellenhof, B., Lichtenegger, H. and Wasle, E. GNSS - Global Navigation Satellite Systems. GPS, GLONASS, Galileo & more. (SpringerWienNewYork, Wien, Austria, 2008).

IGN - Instituto Geográfico Nacional. El Nuevo modelo de geoide para España EGM08-REDNAP (Centro de Observaciones Geodésicas, Instituto Geográfico Nacional, Madrid, 2010).

Junta de Andalucía (2005). Modelo Digital del Terreno de Andalucía. Relieve y Orografía. ISBN: 84-96329-34-8. Sevilla.

Leão, J. W. D., Menezes, P. T. L., Beltrao, J. F. & Silva, J. B. C. (1996). Gravity inversion of basement relief constrained by the knowledge of depth at isolated points. *Geophysics*, 61, 1702–1714, doi:10.1190/1.1444088.

Li, Y and Oldenburg, D.W: (1998) 3-D inversion of gravity data. GEOPHYSICS, VOL. 63, 109–119

Luzón, F., Aoi S., Fäh D. and Sánchez-Sesma F.J. (1995). Simulation of the seismic response of a 2D sedimentary basin: A comparison between the Indirect Boundary Element Method and a Hybrid Technique. Bull. Seism. Soc. Am. Vol. 85, pp. 1501-1506.

Luzón, F., L. Ramírez, F. J. Sánchez-Sesma and A. Posadas (2004). Simulation of the seismic response of sedimentary basins with vertical constant-gradient of velocity. Pure and Applied Geophysics, Vol. 161, 1533-1547.

Luzón, F., F.J. Sánchez-Sesma, J.A. Pérez-Ruiz, L. Ramírez, and A. Pech (2009). In-plane seismic response of inhomogeneous alluvial valleys with vertical gradients of velocities and constant Poisson ratio. Soil Dynamics and Earthquake Engineering, doi:10.1016/j.soildyn.2008.11.007.

Mader, G. and Bilich., A.L. (2012). Absolute Antenna Calibration at the US National Geodetic Survey. AGU Fall Meeting. San Francisco, 3-7 December.

Marin Lechado, C. (2005). Estructura y evolución tectónica reciente del Campo de Dalías y de Níjar en el contexto del límite meridional de las Cordilleras Béticas orientales. PhD Thesis. Universidad de Granada.

Martínez-Martínez, J.M., Azañón, J.M. (1997). Mode of extensional tectonics in the southeastern Betics (SE Spain). Implications for the tectonic evolution of the peri-Alborán orogenic system. *Tectonics* 16, 205-225. doi:10.1029/97TC00157.

Martin-Rosales, W., Pulido-Bosch, A., Vallejos, A. & López-Chicano, M (1996) Extreme rainfall in Campo de Dalías and Southern edge of Sierra de Gádor (Almería). Geogaceta, 20 (6), 1251-1254.

Moritz, H. (1980). Geodetic Reference System 1980, Bulletin Géodésique, 54(3), pp. 251-265.

Oldenburg, D. W. (1974), The inversion and interpretation of gravity anomalies, Geophysics, 39, 526–536, doi:10.1190/1.1440444.

Pedrera, A., Marin-Lechado, C., Galindo-Zaldivar, J., Rodriguez-Fernandez, L.R., Ruiz-Constan, A. (2006): Fault and fold interaction during the development of the Neogene-Quaternary Almeria-Nijar basin (SE Betic Cordilleras). In: C. Moratti, A. Chaluan (eds.), Tectonics of the Western Mediterranean and North Africa. Geological Society, London, Special Publications, 217-230. doi:10.1144/GSL. SP.2006.262.01.13.

Pedrera, A., Galindo-Zaldívar, J., Marín-Lechado, C., García-Tortosa, F.J., Ruano, P., López Garrido, A.C., Azañón, J.M., Peláez, J.A. y Giaconia,F. (2012). Journal of Iberian Geology 38, 191-208.

Pick, M., J. Picha, and V. Vyskôcil (1973), Theory of the Earth's Gravity Field, 538 pp., Elsevier, Amsterdam.

Prieto, J., Sánchez-Sobrino, J.A. and Quirós, R. (2000). Spanish National GPS Reference Station Network (ERGPS). Boletín Real Instituto y Observatorio de la Armada, 3/2000.

Pulido-Bosch, A., Sánchez Martos, F., Martínez Vidal, J.L., Navarrete, F. (1991). Characterization of the overexploitation in the middle and lower Andarax (Almería, Spain). *XXIII IAH Congress Proc.*, Vol. I, 563-569.

Pulido-Bosch, A., Sánchez Martos, F., Martínez Vidal, J.L., Navarrete, F. (1992). Groundwater problems in a semiarid are (Low Andarax River, Almeria, Spain), Environ Geol Water Sci, vol 20, n. 3, 195-204.

Rama Rao, P., K. V. Swamy, and I. V. Radhakrishna Murthy (1999), Inversion of gravity anomalies of three-dimensional density interfaces, Comput. Geosci., 25, 887–896, doi:10.1016/S0098-3004(99)00051-5.

Reamer, S. K., and J. F. Ferguson (1989), Regularized two-dimensional Fourier gravity inversion method with application to the Silent Canyon caldera, Nevada, Geophysics, 54, 486–496, doi:10.1190/1.1442675.

Rama Rao, P., Swamy, K. V. & Radhakrishna Murthy, I. V. (1999). Inversion of gravity anomalies of three-dimensional density interfaces. *Comput. Geosci*., 25, 887–896, doi:10.1016/S0098-3004(99)00051-5.

Sánchez-Martos, F. (1997). Estudio hidrogeoquímico del Bajo Andarax (Almería). PhD Thesis. University of Granada, Spain, 290 pp.

Sanz de Galdeano, C., J. Rodríguez Fernández, and A. C. López Garrido. (1985). A strike-slip fault corridor within the Alpujarra Mountains (Betic Cordilleras, Spain). *GeologischeRundschau,* 74, 641–675.

Sanz de Galdeano, C. & Vera, J.A. (1992). Stratigraphic record and palaeogeographical context of the Neo-gene basins in the Betic Cordillera, Spain. Basin Research, 4: 21-36. http://dx.doi.org/10.1111/j.1365-2117.1992.tb00040.x

Sanz de Galdeano, C., Shanov, S., Galindo-Zaldivar, J., Radulov, A., Nikolov, G. (2010): A new tectonic discontinuity in the Betic Cordillera deduced from active tectonics and seismicity in the Tabernas Basin. *Journal of Geodynamics* 50, 57-66. doi:10.1016/j.jog.2010.02.005.

Tarantola, A. (1988). *The inverse problem theory: Methods for data fitting and model parameter estimation*. Elsevier, Amsterdam, 613 pp.

Torné, M. & Banda, E. (1992). Crustal thinning from the Betic Cordillera to the Alboran Sea. *Geo-Mar. Lett*., 12, 76-81.

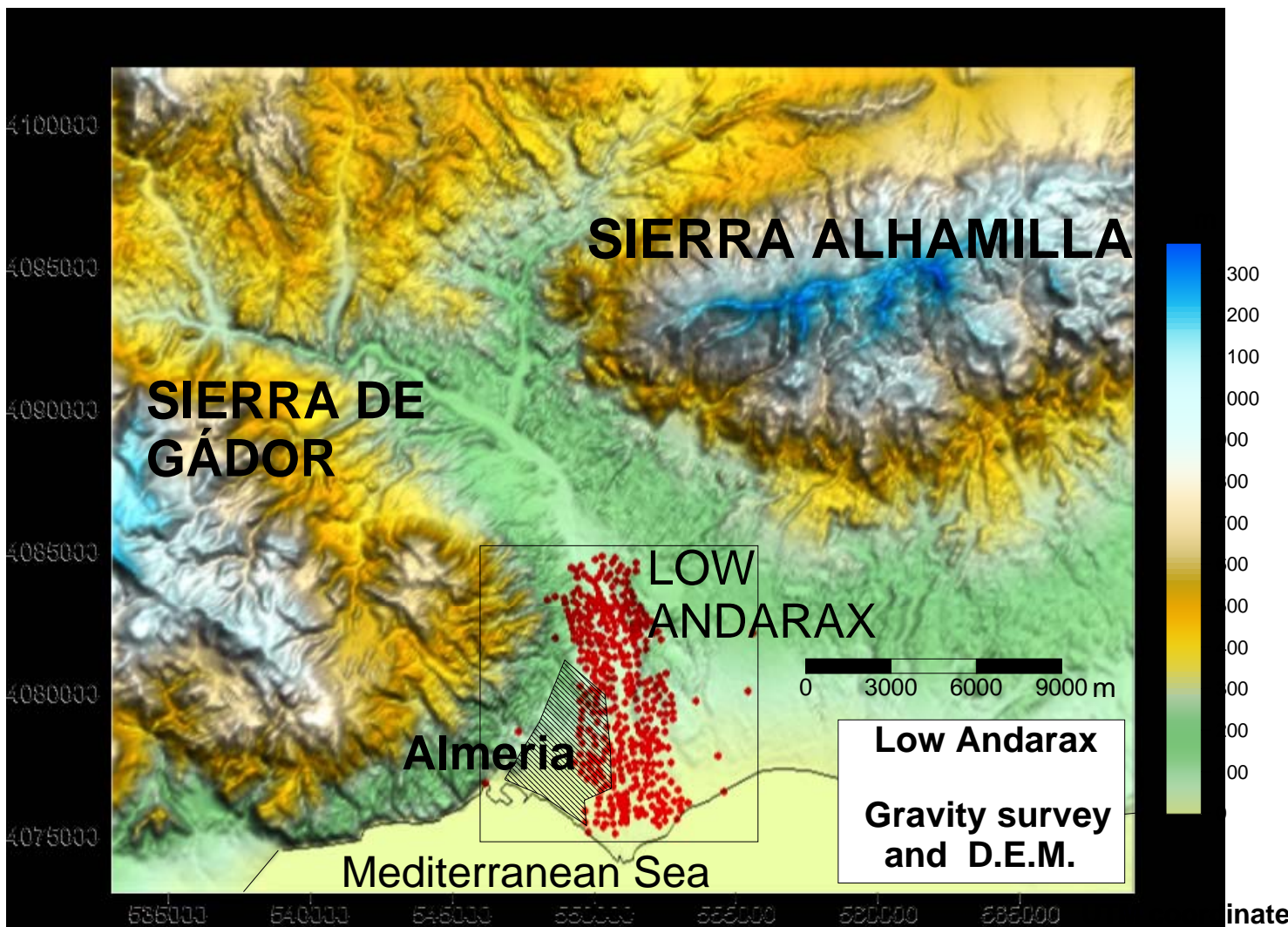Voermans, F. & Baena, J. (1983). Memoria y hoja geológica de Almería (1043) 1:50.000. IGME. Madrid. 53 p.

Figure 1. Sketch of the geographical location of the Low Andarax valley, enclosed by the Mediterranean Sea (south), Sierra Alhamilla (east), and Sierra de Gádor (west). Local D.E.M. and location of the gravity survey. The striped area indicates the city of Almería. The small central rectangle indicates the survey area for the next figures.
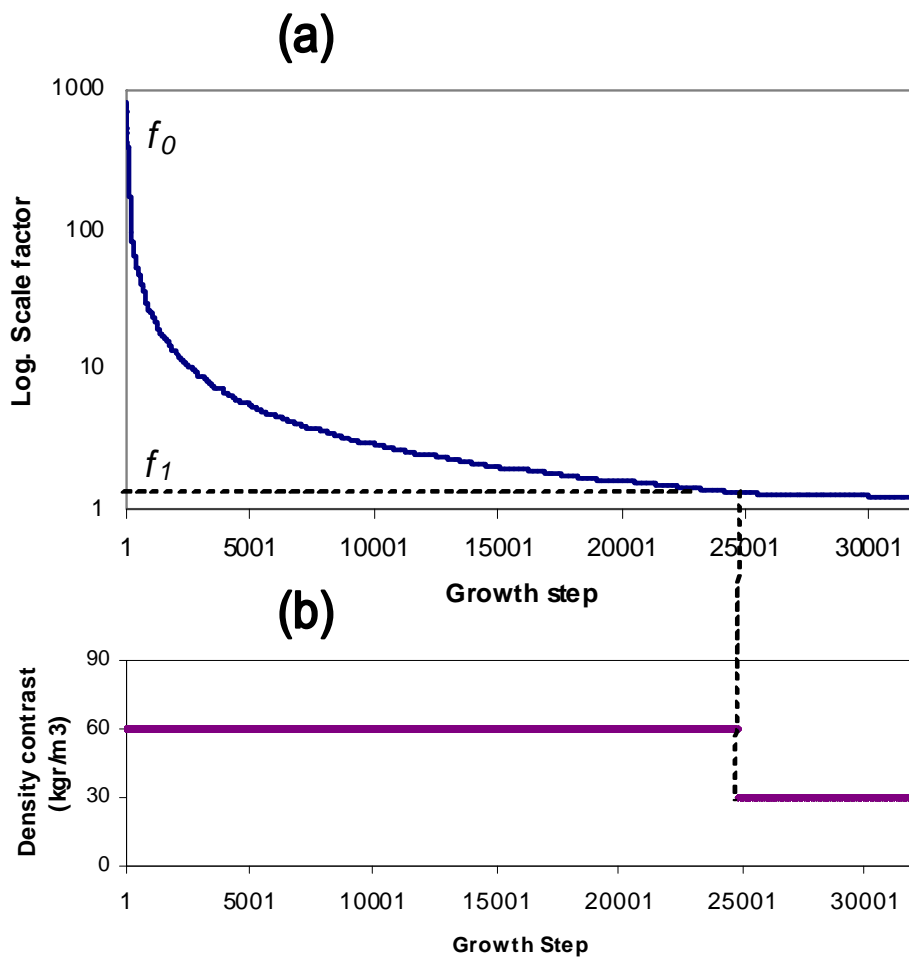
Figure 2. (a) Evolution of the scale factor during the model growth process, (b) stepped

change of the density contrast according the scale evolution to get a stratified inverse model.
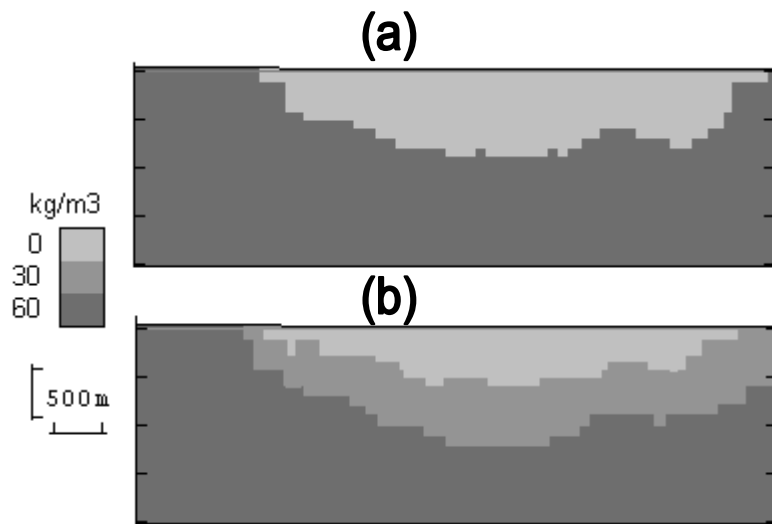
Figure 3. Effect of the stepped change of density contrast across the model growth according

Fig. 2. (a) Constant density contrast. (b) One step density contrast.
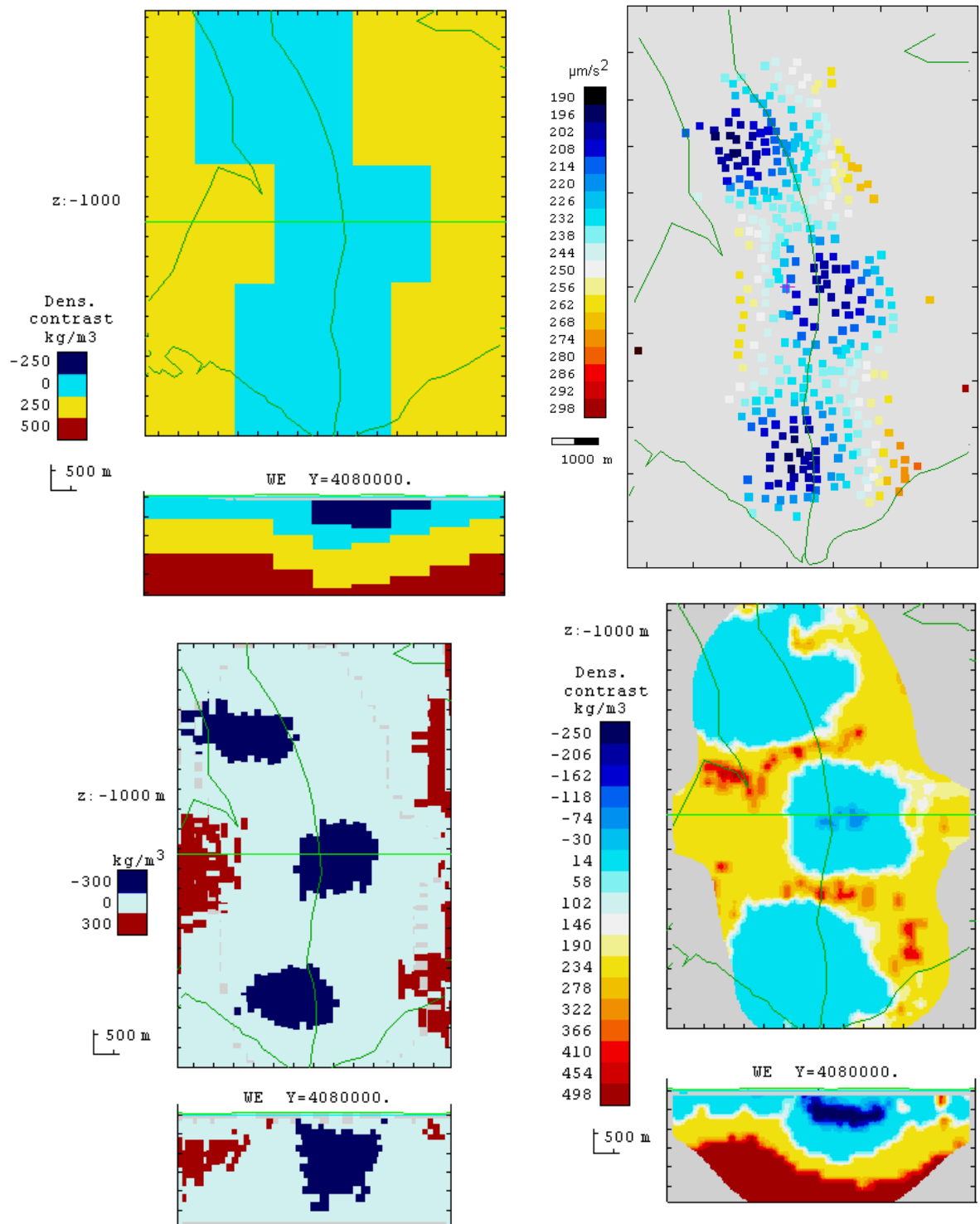
Figure 4. Modelling of a synthetic anomalous structure. (a) 3D systhetic model for a stratified basin estructure. (b) Gravity anomaly corresponding to the systhetic structure for the application gravity points. (c) 3D model obtained by application of the general gravity inversion approach. (d) 3D model obtained by the modified inversion proposed in this paper.
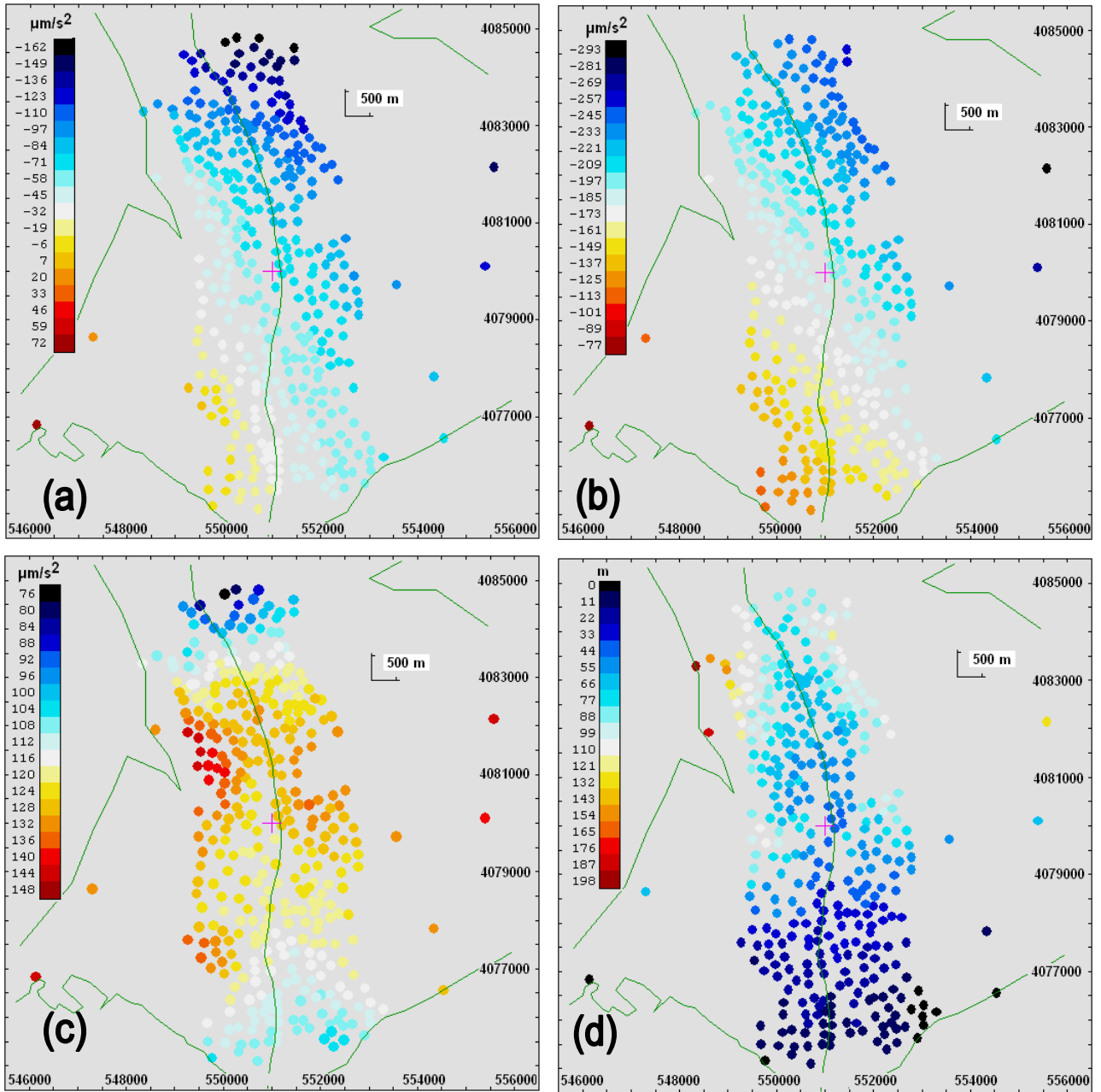
Figure 5. (a) Observed Bouguer anomaly (colour step 1355 μGal). (b) Adjusted linear trend NE-SW (colour step 1146 μGal). (c) Local anomaly (observed anomaly minus trend)(colour step 444 μGal). (d) Elevation of the gravity benchmarks (colour step 11.4 m). UTM coordinates in axes.
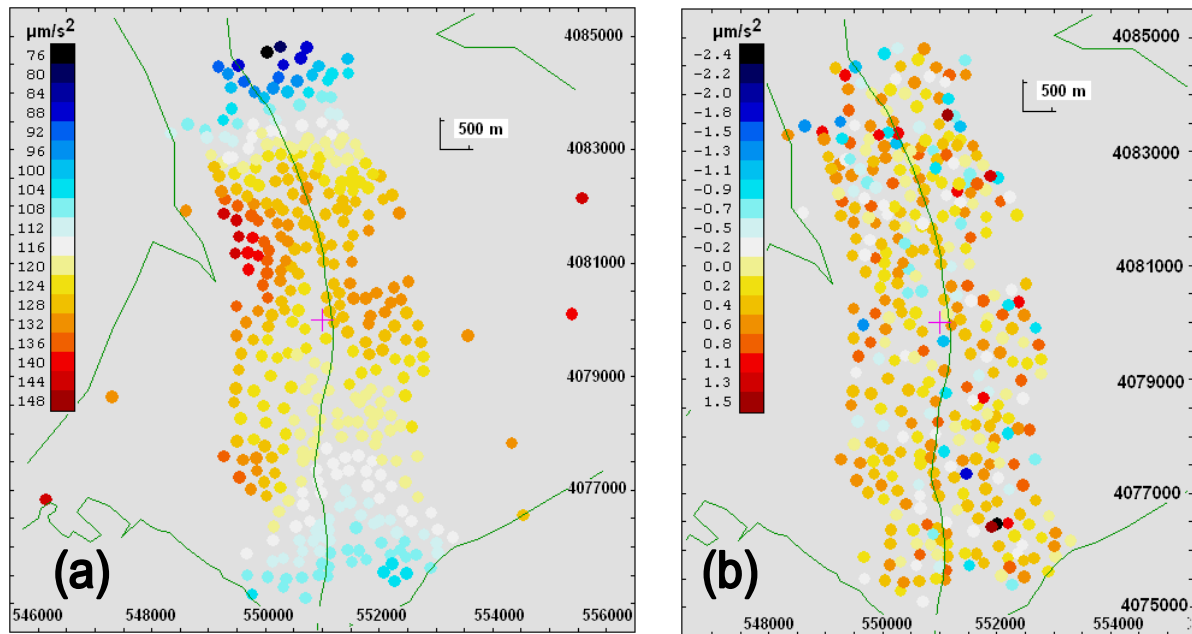
Figure 6. (a) Modelled anomaly after the gravity inversion (colour interval 4.29 μm/s^2). The fit to the observed anomalies (Fig. 4c) is very good. (b) Final residual values after the gravity inversion (colour interval 22 μGal). The standard deviation is about 60 μGal. UTM coordinates in axes.
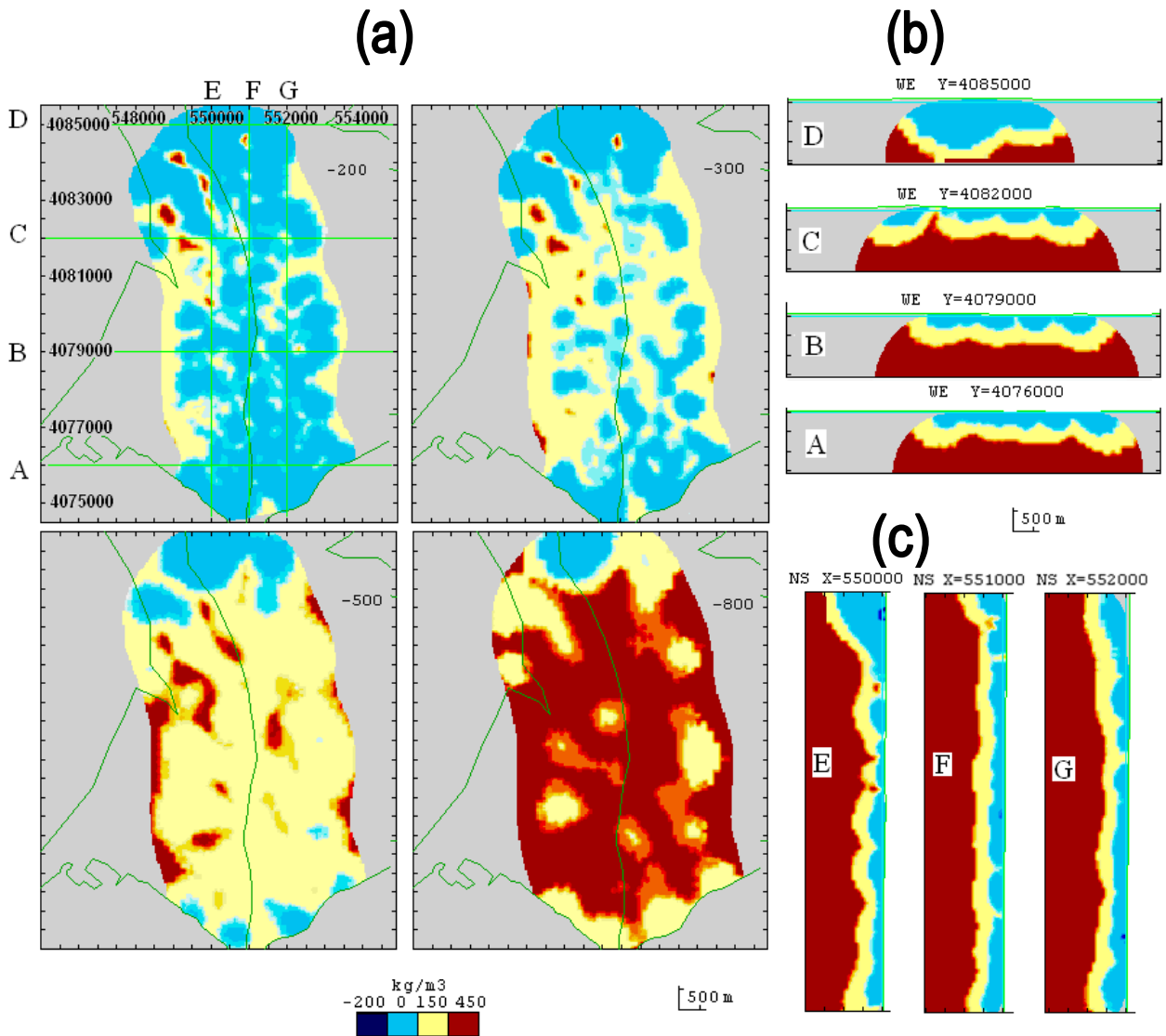
Figure 7. Inverse 3D model for anomalous density. Several cross-sections. (a) Horizontal sections (for 200, 300, 500, 800 m below sea level). (b) WE profiles. (c) NS profiles.
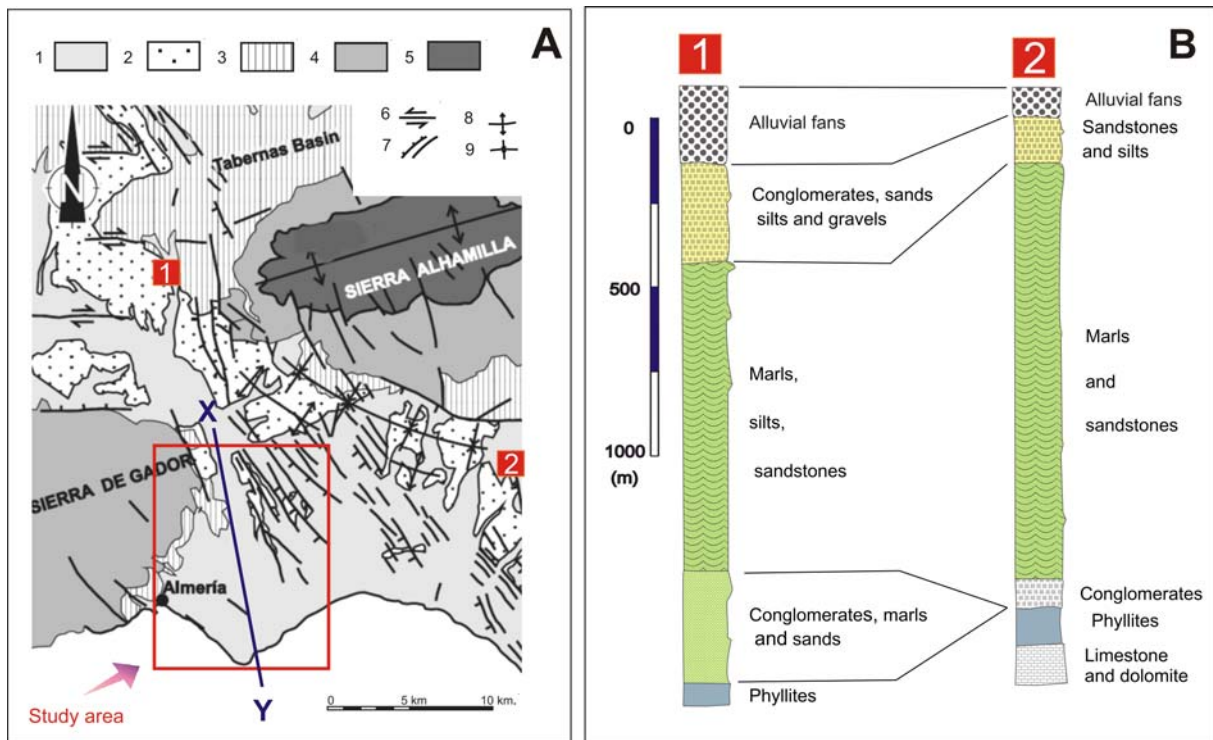
Figure 8. A). Geological map of the Lower Andarax valley. 1: Quaternary detrital alluvial sedimentary deposits. 2: marls, sands and calcarenites (Pliocene), 3: Marls, silts, and sandstones (Middle Miocene?, 4: Alpujárride Complex (phyllites, limestones and dolomites), 5 : Nevado-Filábride complex (metapelites). 6: strike slip fault, 7: Normal Fault, 8: Antiform, 9 : Synform. The cross-section of Figure 8 is marked (X–Y). Modified from Pedrera et al. (2006). B) Synthetic stratigraphic columns and their correlation in different sectors of the Almeria-Nijar Basin. Modified from Marín Lechado (2005).
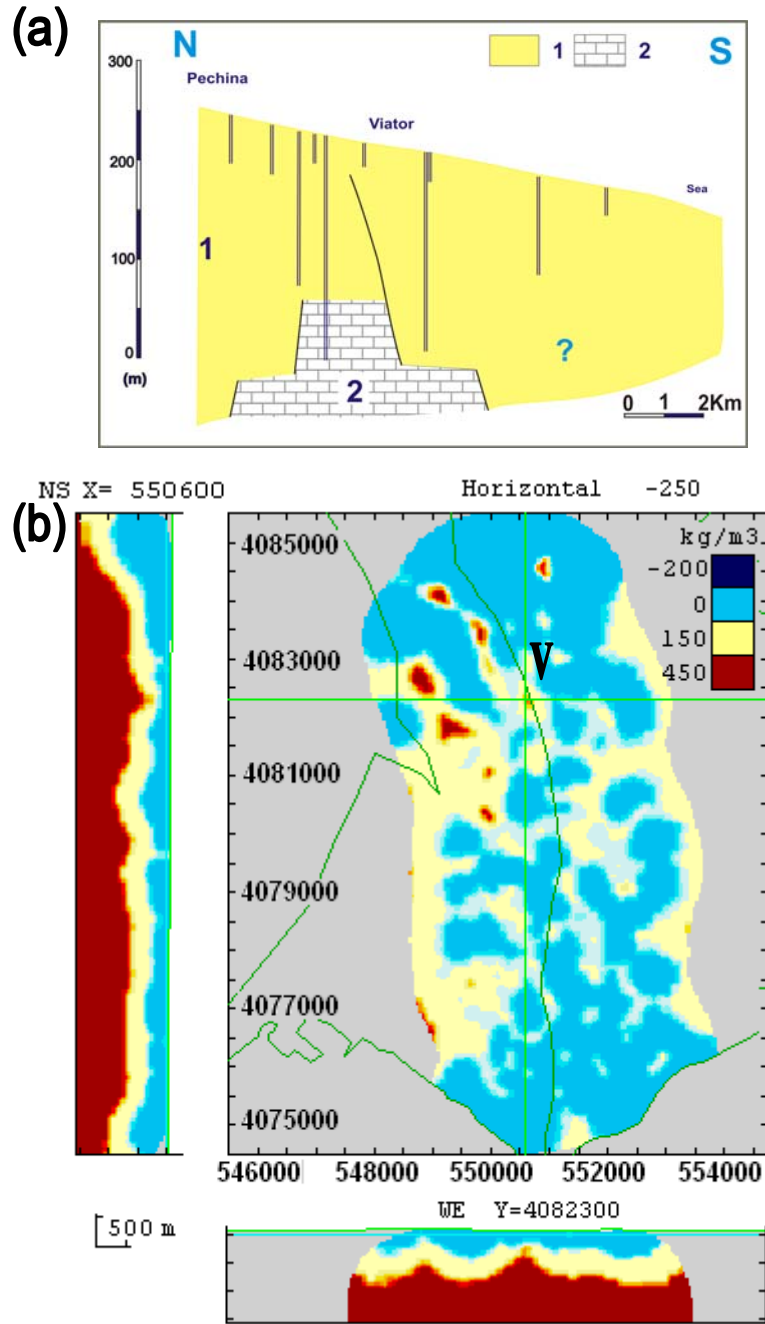
Figure 9. (a) Geological North-South section of the LAV and situation of boreholes. Legend 1: Marls, sandy silts, sands and conglomerates. 2: Limestones and dolomites. (b) Horizontal (250m depth) and vertical (NS and WE) cross-sections of the density model inverted from the gravimetric survey, showing a high density anomaly in Viator area. UTM coordinates.
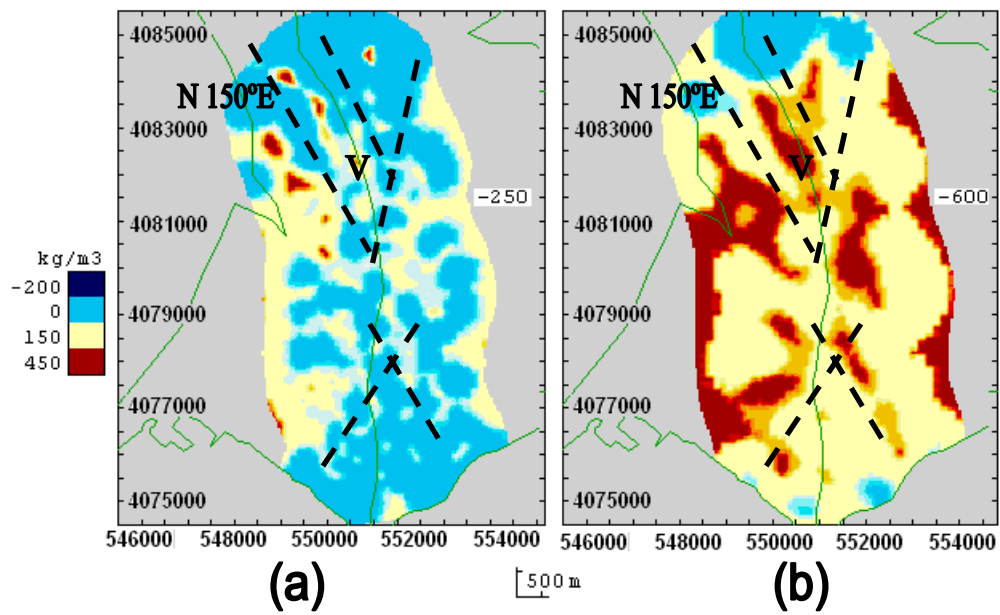
Figure 10. Some structural alignments (mainly N150ºE) of lows in the inverse model. (a) Shallow section at 250 m depth below sea level. (b) Deep section at 600 m. Letter V indicates location of Viator village UTM coordinates.